Mon. Not. R. Astron. Soc. **000**, 1–11 (2016) Printed 22 July 2016 (MN LATEX style file v2.2)

Viscous time lags between starburst and AGN activity

Marvin Blank[1⋆] and Wolfgang J. Duschl[1,2⋆]
[1] *Institut für Theoretische Physik und Astrophysik, Christian-Albrechts-Universität zu Kiel, Leibnizstr. 15, D-24118 Kiel, Germany*
[2] *Steward Observatory, The University of Arizona, 933 N. Cherry Ave., Tucson, AZ 85721, USA*

arXiv:1607.06365v1 [astro-ph.GA] 21 Jul 2016

22 July 2016

ABSTRACT
There is strong observational evidence indicating a time lag of order of some 100 Myr between the onset of starburst and AGN activity in galaxies. Dynamical time lags have been invoked to explain this. We extend this approach by introducing a viscous time lag the gas additionally needs to flow through the AGN's accretion disc before it reaches the central black hole. Our calculations reproduce the observed time lags and are in accordance with the observed correlation between black hole mass and stellar velocity dispersion.

Key words: galaxies: active – galaxies: formation – galaxies: interactions – galaxies: nuclei – quasars: general – galaxies: starburst.

1 INTRODUCTION

Motivated by, for instance, observed correlations between the mass of an AGN's central black hole and the host galaxy's velocity dispersion (e.g., Gebhardt et al. 2000) and between black hole mass and bulge mass (e.g., Kormendy & Richstone 1995), there is an ongoing debate whether, and if so, how starbursts and AGN are connected to each other.

Di Matteo et al. (2005), for instance, explain such correlations as due to a thermal AGN feedback that heats the gas of the galaxy and thus prevents further star formation and AGN activity: More massive galaxies have a deeper gravitational potential well, thus the black hole has to gain more mass before its luminosity is capable of expelling the gas from the galaxy and quenching star formation and AGN activity. This then leads to the velocity dispersion and the bulge mass, resp., to be related to the black hole mass. In these simulations starburst and AGN activity occur simultaneously, but recent observations show that AGN activity may be delayed with regard to star formation activity by time-scales of 50–250 Myr (e.g., Davies et al. 2007; Schawinski et al. 2009; Wild et al. 2010).

Hopkins (2012) argues that such a time lag can occur for purely dynamical reasons. His high spatial resolution simulations of galaxy mergers show first an inward motion of gas towards the dynamical centre giving rise to (a burst of) star formation. In these models, the gas flowing further inwards can do so only by losing angular momentum by gravitational instabilities. This, in turn, gives rise to a time lag between star formation and AGN activity.

⋆ E-mail: mblank@astrophysik.uni-kiel.de (MB); wjd@astrophysik.uni-kiel.de (WJD)

We extend this idea by modelling the loss of angular momentum and the ensuing inflow in the framework of an accretion disc scenario. Thus the time lag between starburst and AGN activity consists of a dynamical lag given by the time span the gas needs to reach the accretion disc and a subsequent viscous lag given by the time span the gas needs to flow through the accretion disc until it reaches the black hole.

In Section 2 we explain our numerical methods and the setup of the merger event that is, in this scenario, responsible for the inflow of gas to the newly forming galactic centre. In Section 3 we present and discuss the general picture that results from our calculations. As our model depends on a number of parameters, we perform a parameter study in Section 4 to show the robustness of our results against parameter changes. In Section 5 we summarise our findings.

2 NUMERICAL METHODS

We simulate galaxy collisions using the TreeSPH code GADGET-2 (Springel 2005). Radiative cooling of an optically thin primordial gas in ionization equilibrium is taken into account following Katz et al. (1996). Additionally we include star formation, AGN evolution and AGN feedback as described in the following subsections.

2.1 Star formation

Following Scannapieco et al. (2005) a gas particle is considered for star formation if its density ρ exceeds a critical density ρ_{crit} and it is in a converging flow ($\operatorname{div} v < 0$). Then

© 2016 RAS

a star particle is created with a probability

$$p = \frac{m}{m_*}\left[1 - \exp\left(-\frac{c_{\rm eff}\,\Delta t}{t_{\rm g}}\right)\right] \quad (1)$$

(see Springel & Hernquist 2003) where m is the gas particle's mass, $m_* = m_0/N_{\rm g}$ the mass of the star to be formed, m_0 the initial gas particle mass, $N_{\rm g}$ the number of stars that can be formed from one gas particle, $c_{\rm eff}$ the star forming efficiency, Δt the respective time step of the code and $t_{\rm g} = \sqrt{3\pi/32G\rho}$ the free-fall time of the gas particle. If $m < 1.5 \times m_*$, condition (1) is dropped and the gas particle is directly converted into a star particle. Gas particles can only reduce their mass due to star formation. In our simulations star particles are collisionless particles and interact with other particles only via gravitational forces. For the star forming efficiency we use a value of $c_{\rm eff} = 0.1$ following Katz (1992). The parameter $N_{\rm g}$ determines the numerical resolution of the star formation rate, like Scannapieco et al. (2005) we use a value of $N_{\rm g} = 2$. We furthermore set $\rho_{\rm crit} = 4.5 \times 10^8\ {\rm M_\odot\,kpc^{-3}}$.

With these parameters the simulation of an isolated galaxy characterized by the parameters given in Table 1 gives an average star formation rate of $0.26\,{\rm M_\odot\,yr^{-1}}$. This value fits well with the star formation rate that is expected in such a galaxy: According to Kennicutt (1998) the star formation rate of an isolated galaxy can be estimated as

$$\dot{M}_{\rm SFR} = 0.017\frac{M_{\rm gas}}{\tau_{\rm dyn}} \quad (2)$$

with the total gas mass $M_{\rm gas}$ and the dynamical time-scale at the half gas-mass radius $\tau_{\rm dyn}$. According to this equation an isolated galaxy characterized by the parameters given in Table 1 has a star formation rate of $0.3\,{\rm M_\odot\,yr^{-1}}$.

In our simulations star formation takes place only in the host galaxy and not in the accretion disc that surrounds the central black hole. It is currently highly debated if such accretion discs can be subject to star formation. On the one hand, the accretion disc's viscosity might heat the gas up to temperatures that prevent the gravitational collapse of the gas and thus subsequent star formation. On the other hand gravitational fragmentation of a self-gravitating accretion disc might favor gravitational collapse and thus trigger star formation. Star formation in the accretion disc will subsequently lead to stellar feedback processes, which can potentially clear the central region of gas and thus prevent accretion of material towards the black hole. However, as this topic is still a subject of intense debate we will neglect star formation in the accretion disc in our simulations. Stellar feedback is not included in our simulations, we leave the study of these effects for later investigations.

2.2 Modeling the AGN

The AGN is represented by an *accretion disc particle* (ADP) as introduced by Power et al. (2011), which interacts with its environment only via gravitational forces, accretion of gas particles and AGN feedback.

The black hole growth rate is calculated via a subgrid model: The ADP contains a black hole and an accretion disc, the mass accreted by the ADP is added to the outer rim of the accretion disc, from where it is accreted towards the black hole. The details of this accretion process are described in the next subsection.

We use the implementation of Jappsen et al. (2005) to describe the accretion of gas particles, but as suggested in Power et al. (2011) gas particles are accreted only if their distance to the ADP falls below the ADP's accretion radius $R_{\rm acc}$, which is a free parameter.

Wurster & Thacker (2013) investigate the impact of various parameters in the ADP model in simulations of Milky Way-sized galaxy mergers and explore how to set $R_{\rm acc}$ accordingly. Their simulations produce unphysical results when $R_{\rm acc} \leqslant 0.02\,h_{\rm min}$ or $R_{\rm acc} \geqslant 0.2\,h_{\rm min}$, where $h_{\rm min}$ is the minimum smoothing length. Their definition of physical or unphysical is based on, besides analyzing the structural evolution of the galaxy merger, how close the merger remnant lies on the $M_{\rm BH}$-σ correlation. For very small values of $R_{\rm acc}$ the accretion rate of the black hole is underestimated which leads to black hole masses that are too small, whereas very large values of $R_{\rm acc}$ lead to black hole masses that are too large.

In our simulations the minimum smoothing length is $h_{\rm min} = 250\,{\rm pc}$ and thus in our reference model $R_{\rm acc} = 0.8\,h_{\rm min}$. This is much larger than allowed by the analysis of Wurster & Thacker (2013). However, our simulations include AGN feedback in the form of a wind that reduces the accretion rate of the black hole and thus the final black hole mass. Therefore our simulations produce black hole masses that are in agreement with the observed $M_{\rm BH}$-σ correlation, making an accretion radius of $R_{\rm acc} = 200\,{\rm pc}$ for our reference model a reasonable choice.

2.3 Evolution of the AGN

We assume the accretion disc that is hosted by the ADP to be rotationally symmetric and geometrically thin, furthermore we assume the gravitational potential to change slowly enough so that in the following we can neglect its explicit time derivative. This then leads to a single equation that describes the time dependent evolution of the accretion disc's surface density Σ (see, e.g., Pringle 1981):

$$\frac{\partial\Sigma}{\partial t} + \frac{1}{s}\frac{\partial}{\partial s}\left[\frac{\frac{\partial}{\partial s}\left(\nu\Sigma s^3\frac{\partial\omega}{\partial s}\right)}{\frac{\partial}{\partial s}\left(s^2\omega\right)}\right] = 0 \quad (3)$$

Here s is the distance to the central black hole. ω is the angular frequency which we calculate through a balance between gravitational and centrifugal forces. ν is the viscosity of the gas, which we parametrize such that the viscous time-scale is related to the dynamical time-scale via $t_{\rm visc} = \xi t_{\rm dyn}$ with a constant parameter ξ of order 10^2–10^3 (Duschl et al. 2000)[1].

We carry out the time integration of equation (3) by applying an implicit Crank-Nicolson finite differences scheme (Crank et al. 1947). The radial calculation domain extends from an inner radius $s_{\rm in}$ to the disc's initial outer radius $s_{\rm out,0}$. We set $s_{\rm in} = 10^{-3}\,{\rm pc}$ for all calculations presented in this paper, tests showed that moderate variations of this value have almost no effect on the results. Between the inner

[1] Duschl et al. (2000) use the parameter $\beta = \xi^{-1}$, which is of order 10^{-3}–10^{-2}.

and the outer radius 25 grid points are distributed logarithmically.

For solving equation (3) with the aim of obtaining the mass supply rate $\dot{M}_\mathrm{d}$ from the disc, an initial condition for the surface density is necessary, for simplicity we assume a constant density distribution $\Sigma_0 = M_{\mathrm{d},0}/(\pi s_{\mathrm{out},0}^2)$, with the initial disc mass $M_{\mathrm{d},0}$ and the disc's initial outer radius $s_{\mathrm{out},0}$. In addition to being a simple initial condition, it guarantees that in the disc viscous processes dominate the time-scales as initially most of the disc's mass is at larger radii.

Thus for our disc model we have to specify four parameters: the ratio of viscous time-scale to dynamical time-scale ξ, the initial black hole mass $M_{\mathrm{BH},0}$, the initial disc mass $M_{\mathrm{d},0}$ and the disc's initial outer radius $s_{\mathrm{out},0}$ with the latter corresponding to the ADP's accretion radius R_acc. We use $\xi = 250$, $M_{\mathrm{BH},0} = 5 \times 10^5\,\mathrm{M}_\odot$ and $M_{\mathrm{d},0} = 5 \times 10^5\,\mathrm{M}_\odot$. The initial masses of the black hole and the accretion disc have almost no effect on the results as long as they are not too large. We furthermore set $R_\mathrm{acc} = 200\,\mathrm{pc}$ where viscous processes start to play a dominant role for the accretion of material onto the black hole.

2.4 AGN feedback

For modeling the AGN feedback we follow Debuhr et al. (2011, 2012). There the AGN's radiation causes a force

$$\dot{p}_\mathrm{rad} = \tau \frac{L}{c} \tag{4}$$

on the surrounding gas where $L = \eta c^2 \dot{M}_\mathrm{BH}$ is the AGN's luminosity, $\dot{M}_\mathrm{BH}$ the black hole accretion rate and η the accretion efficiency, which is $\sim 10^{-1}$ for standard accretion discs (Shakura & Sunyaev 1973).

τ is the wavelength-averaged optical depth of the gas that surrounds the AGN and a free parameter, following Debuhr et al. (2011) we use a value of $\tau = 25$.

The AGN additionally drives a wind adding a force

$$\dot{p}_\mathrm{w} = \tau_\mathrm{w} \frac{L}{c} \tag{5}$$

to the surrounding gas where τ_w is a further free parameter of the model determining the total momentum flux in the wind, we choose a value of $\tau_\mathrm{w} = 3$ to normalize the M_BH-σ correlation (see Section 3).

Assuming the wind to be launched at a speed v_w, equation (5) yields its mass flow

$$\dot{M}_\mathrm{w} = \tau_\mathrm{w} \frac{L}{c v_\mathrm{w}} = \tau_\mathrm{w} \eta \frac{c}{v_\mathrm{w}} \dot{M}_\mathrm{BH}\,. \tag{6}$$

Here we use $v_\mathrm{w} = 10^4\,\mathrm{km\,s^{-1}}$ following Debuhr et al. (2012).

As thus not all of the mass that is made available by the accretion disc enters the black hole, its accretion rate must be reduced accordingly

$$\dot{M}_\mathrm{BH} = \dot{M}_\mathrm{d} - \dot{M}_\mathrm{w} \tag{7}$$

which yields, considering equation (6),

$$\dot{M}_\mathrm{BH} = \frac{\dot{M}_\mathrm{d}}{1 + \tau_\mathrm{w} \eta c v_\mathrm{w}^{-1}}\,. \tag{8}$$

Following, e.g., Debuhr et al. (2011, 2012), Di Matteo et al. (2005), Springel et al. (2005) we furthermore limit the black hole accretion rate to the Eddington limit

$$\dot{M}_\mathrm{Edd} = \frac{M_\mathrm{BH}}{\tau_\mathrm{S}} \tag{9}$$

(Eddington 1921). Here M_BH is the black hole mass and $\tau_\mathrm{S} = \eta \times 4.5 \times 10^8\,\mathrm{yr}$ the Salpeter time-scale (Salpeter 1964).

Each time step the total amount of mass $\dot{M}_\mathrm{w}\Delta t$ and momentum $(\dot{p}_\mathrm{rad} + \dot{p}_\mathrm{w})\Delta t$ made available by the AGN are calculated and equally distributed among the SPH-particles within a radius $2R_\mathrm{acc}$.

Table 1. Parameters of our reference model, a galaxy with these parameters has a scale radius of 3.8 kpc.

virial velocity	v_{200}	$160\,\mathrm{km\,s^{-1}}$
mass fraction of the disc	m_d	0.041
mass fraction of the bulge	m_b	0.0137
mass fraction of the gas	f_g	0.3
scale height of the disc[a]	f_d	0.2
scale radius of the bulge[a]	f_b	0.1
halo concentration	c_halo	15
spin parameter of the halo	λ	0.05
angular momentum fraction of the disc	j_d	0.041

[a] in fractions of the disc's scale radius

2.5 Initial conditions and parameters

We model our galaxies as described by Springel & White (1999) and Springel (2000) based on the analytical model of Mo et al. (1998).

A galaxy is characterized via a virial velocity v_{200} that corresponds to a virial mass

$$M_{200} = \frac{v_{200}^3}{10 G H_0} \tag{10}$$

with the gravitational constant G and the Hubble constant[2] H_0.

A fraction m_d of the virial mass forms a thin (galactic) disc with a profile

$$\rho_\mathrm{d}(R,z) = \rho_0 \exp\left(-\frac{R}{R_\mathrm{d}}\right) \mathrm{sech}^2\left(\frac{z}{z_0}\right)\,. \tag{11}$$

The disc's scale height z_0 is a fraction f_d of the disc's scale radius R_d. A fraction f_g of the disc consists of gas, the rest consists of old stars. Another fraction m_b of the virial mass forms a spherical bulge with a Hernquist (1993) profile whose scale radius is again a fraction f_b of the disc's scale radius R_d.

The rest of the total mass forms a dark matter halo with a Navarro et al. (1996, 1997) profile whose scale radius is a fraction c_halo^{-1} of the virial radius where c_halo is the halo concentration. The angular momentum of the halo is characterized by a dimensionless spin parameter λ. Setting the disc's angular momentum to a fraction j_d of the halo's angular momentum determines the disc's scale radius. Thus the galaxy model depends on nine parameters, which we list in Table 1 for our reference model. The particle's positions

[2] We use a value of $H_0 = 70\,\mathrm{km\,s^{-1}\,Mpc^{-1}}$ throughout this paper.

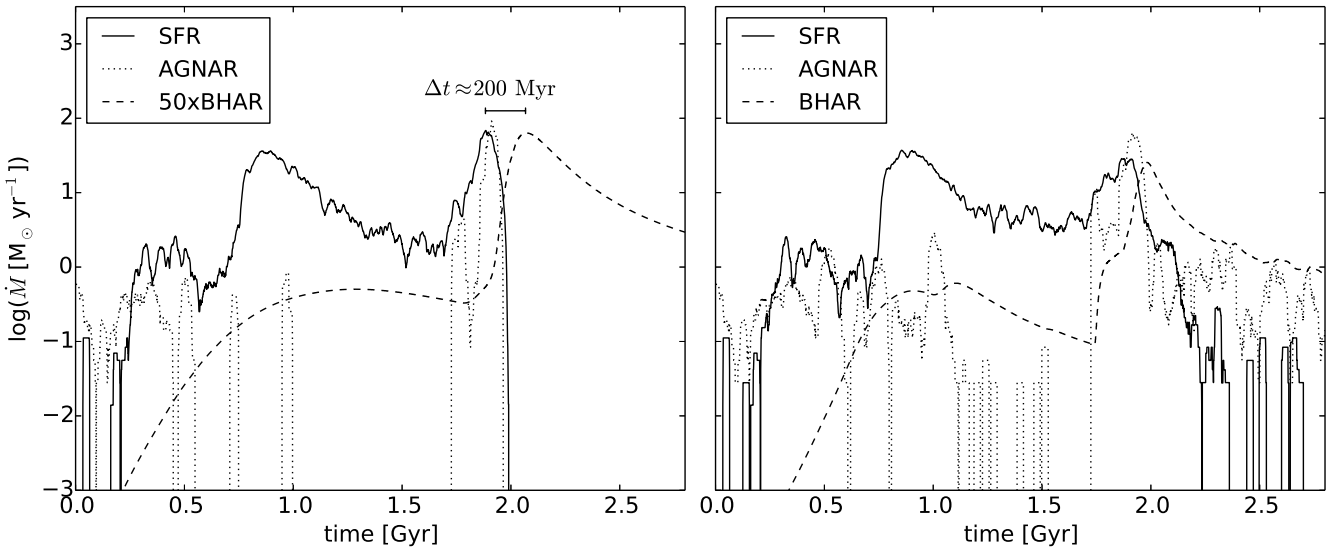

Figure 1. Star formation rate (SFR), accretion rate of the AGN (AGNAR) and black hole accretion rate (BHAR) as functions of time. Left: with AGN feedback, right: without AGN feedback.

are initialized according to the above mentioned mass distributions, the particle's velocities are initialized according to the solution of the Boltzmann equation. For details on this procedure we refer to Springel & White (1999).

Each galaxy consists of 30 000 particles for the halo, 10 000 for the bulge, 20 000 for the stellar disc and 20 000 for the gaseous disc.

According to Khochfar (2003) merging dark matter halos are mostly on parabolic orbits, we therefore set the galaxies on a parabolic orbit with a periapsis of $r_\mathrm{p} = 5$ kpc and an initial distance of $r_0 = 300$ kpc. In one of the galaxy's centres we place an ADP with mass 10^6 $\mathrm{M}_\odot$ (sum of initial black hole mass and initial disc mass).

Test calculations showed that simulations where both galaxies contain an ADP produce about the same results. We prefer simulations with only one galaxy hosting an ADP because otherwise we would have to introduce a number of additional assumptions and parameters to account for the merging of the two ADP.

The gravitational softening length for the halo particles is 0.8 kpc and 0.5 kpc for all other particles. The minimum smoothing length is set to half the gravitational softening length.

3 THE GENERAL PICTURE

The time evolution of the merger event brings the galaxies to their first passage ~ 0.7 Gyr after the start of the simulation, they finally merge at 1.8 Gyr and form a gas-poor elliptical galaxy. Fig. 1 shows the star formation rate (SFR), the accretion rate of the AGN (AGNAR) and the black hole accretion rate (BHAR) as functions of time. We simulated the merger event once with and once without AGN feedback.

The merging event drives huge amounts of gas towards the centre of the new forming merged galaxy where it causes a starburst with a lifetime of 200–300 Myr (in accordance with the observations of Wild et al. 2010 and the simulations of Di Matteo et al. 2005) and feeds the AGN.

After being devoured by the ADP the gas has to flow through the accretion disc on a viscous time-scale that corresponds to a time lag of approx. 200 Myr between the peak of the AGNAR and the peak of the BHAR, resulting in a time lag between starburst and AGN activity that is in agreement with observations (e.g., Wild et al. 2010).

This time lag does not render AGN feedback ineffective. Although the BHAR peaks much later than the SFR and the AGNAR, the feedback already starts working well before the BHAR peaks. This is evident when comparing the simulations with and without feedback in Fig. 1, where AGN feedback clearly quenches the SFR and the AGNAR.

However, during the time lag until the onset of AGN activity huge amounts of mass are inserted into the accretion disc. Thus the BHAR is not quenched by the AGN feedback, the AGN continues evolving for some time after the galaxies have merged. But due to the feedback the BHAR is reduced by approx. one order of magnitude, compared with the simulation without feedback. Feedback given to the accretions disc's gas is parametrized by the reduction of the black hole accretion rate according to equation (8).

To check the agreement of our model with the observed correlation between black hole mass and stellar velocity dispersion (M_BH-σ correlation) we repeat the calculations for different virial masses. The critical density for the onset of star formation is rescaled according to

$$\rho_{\mathrm{crit},*} = \frac{M_{200,*}}{M_{200,\mathrm{ref}}} \rho_{\mathrm{crit,ref}} \tag{12}$$

where $\rho_{\mathrm{crit},*}$ and $M_{200,*}$ are the critical density and the virial mass of the respective model and $\rho_{\mathrm{crit,ref}}$ and $M_{200,\mathrm{ref}}$ are the critical density and the virial mass of the reference model that we have specified in the previous sections. The rescaling of the critical density is necessary to compensate for the changing resolution that arises from a constant particle number and a changing galaxy mass. Tests that were conducted in the same manner than described in Section 2.1 show that the simulated star formation rate and the star formation rate implied by equation (2) differ by less than

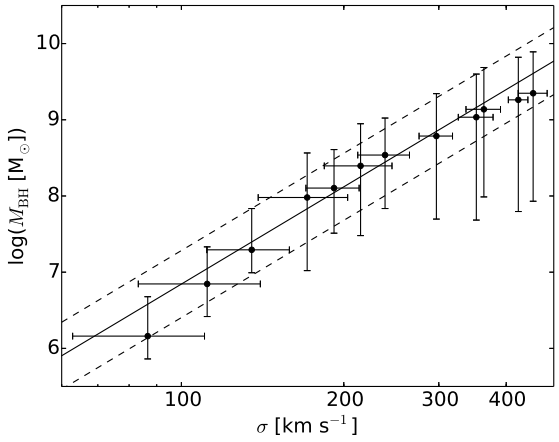

Figure 2. Black hole mass $M_{\rm BH}$ as function of the galaxy's stellar velocity dispersion σ. The dots indicate the black hole mass at the time the black hole accretion rate (BHAR) reaches its maximum value. The horizontal bars indicate the error of σ, the vertical bars indicate the range of black hole mass from the time of the end of the starburst to the time the BHAR decreases to 0.3 % of its Eddington rate. The solid line indicates the observed $M_{\rm BH}$-σ correlation with intrinsic scatter (dashed lines) according to Gültekin et al. (2009).

a factor of two. The initial masses of black hole and accretion disc and the acccretion radius are rescaled in the same manner.

Fig. 2 shows the mass of the black hole at the time the BHAR reaches its maximum value as function of the stellar velocity dispersion of the resulting elliptical galaxy, on how to calculate the latter we refer to Debuhr et al. (2011). The results are consistent with the observed correlation from Gültekin et al. (2009) indicated by the solid line. As the black hole continues growing after the galaxies have merged we additionally plot the range of black hole mass from the time of the end of the starburst to the time the BHAR decreases to 0.3 % of its Eddington rate. According to Beckert & Duschl (2002) the radiation efficiency of accretion discs declines steeply below this rate, making it increasingly unlikely to detect those discs. Our results suggest that this continuing evolution of the black hole mass may contribute to the large scatter of the observed $M_{\rm BH}$-σ correlation that is indicated by the dashed lines in Fig. 2.

4 PARAMETER STUDY

As our simulations depend on a number of parameters, some of which are not well constrained by observations, we will perform a parameter study in this chapter to test the robustness of our results against parameter changes.

However, we only use our reference model with $v_{200} = 160\,{\rm km\,s^{-1}}$ for the parameter study and do not investigate the effects of parameter changes on the $M_{\rm BH}$-σ correlation. The latter has been done by several authors, e.g., Debuhr et al. (2012, 2011); Johansson et al. (2009); Di Matteo et al. (2005).

For our study we choose the following parameters: the accretion radius $R_{\rm acc}$, the viscosity parameter ξ and the feedback parameters $\tau_{\rm r}$ and $\tau_{\rm w}$. The chosen values of these parameters are summarized in Table 2. We furthermore investigate the effect of varying the resolution of our simulations.

Table 2. Parameters used in our parameter study.

$R_{\rm acc}$ (pc)	100, 150, 250, 300, 350, 400
ξ	100, 125, 400, 500, 800, 1000
$\tau_{\rm r}$	19, 21, 23, 27, 29, 31
$\tau_{\rm w}$	1, 2, 4, 5, 6, 7

We analyze the SFR, BHAR and AGNAR versus time, which are plotted in Fig. 3 for different accretion radii $R_{\rm acc}$, in Fig. 4 for different viscosity parameters ξ and in Figs. 5 and 6 for different feedback parameters $\tau_{\rm r}$ and $\tau_{\rm w}$, respectively. All simulations produce a starburst and a peak in AGN activity as shown for our reference model, and produce a time lag between these two phenomena of order of some 100 Myr. Furthermore all simulations are consistent with the $M_{\rm BH}$-σ correlation in the sense that the black hole mass at the time the BHAR peaks lies within the intrinsic scatter of the observed correlation of Gültekin et al. (2009).

However, the simulations with $R_{\rm acc} = 350\,{\rm pc}$ and $R_{\rm acc} = 400\,{\rm pc}$ show only a very weak peak in the BHAR. In these simulations the first close encounter of both galaxies already drives a huge amount of mass towards the centre that is accreted by the ADP, as a result there is not much gas left for accretion when the galaxies finally merge. According to Wurster & Thacker (2013) an accretion radius that is too large for the adopted level of resolution produces a BHAR that is too high, which happens here after the first encounter of the galaxies.

We also investigate the time lag between starburst and AGN activity. The time of the starburst we roughly estimate by determining the time the SFR reaches its maximum value, likewise the time of AGN activity equals the time the BHAR reaches its maximum value. Both events are represented by vertical lines in Figs. 3–6. The difference of these two times, i.e., the time lag between starburst and AGN activity, is shown in Fig. 8 for all parameters of our parameter study.

As this time lag is a viscous time-scale, it is related to the orbital time-scale t_ω via

$$t_\nu = \xi t_\omega = 2\pi\xi\sqrt{\frac{R^3}{GM}} \tag{13}$$

where R can be approximated by the accretion radius $R_{\rm acc}$ and M by the sum of black hole mass and the mass of the accretion disc. Fig. 8 confirms that the time lag increases with increasing $R_{\rm acc}$ and with increasing ξ, and does not change significantly with $\tau_{\rm r}$ and $\tau_{\rm w}$.

Observations show time lags of about 50–250 Myr which are reproduced by most of our simulations, but a few of our simulations produce time lags that have values of up to 550 Myr. Such large time lags have not been directly observed yet. However, Wild et al. (2010) only measure the average time lag of a sample of about 400 galaxies with a result of 250 Myr, thus some of the galaxies involved will have time lags that exceed this average value.

Fig. 7 shows SFR, BHAR nad AGNAR versus time for different levels of resolution. We increase the number of particles by a factor of two and a factor of four, respectively.

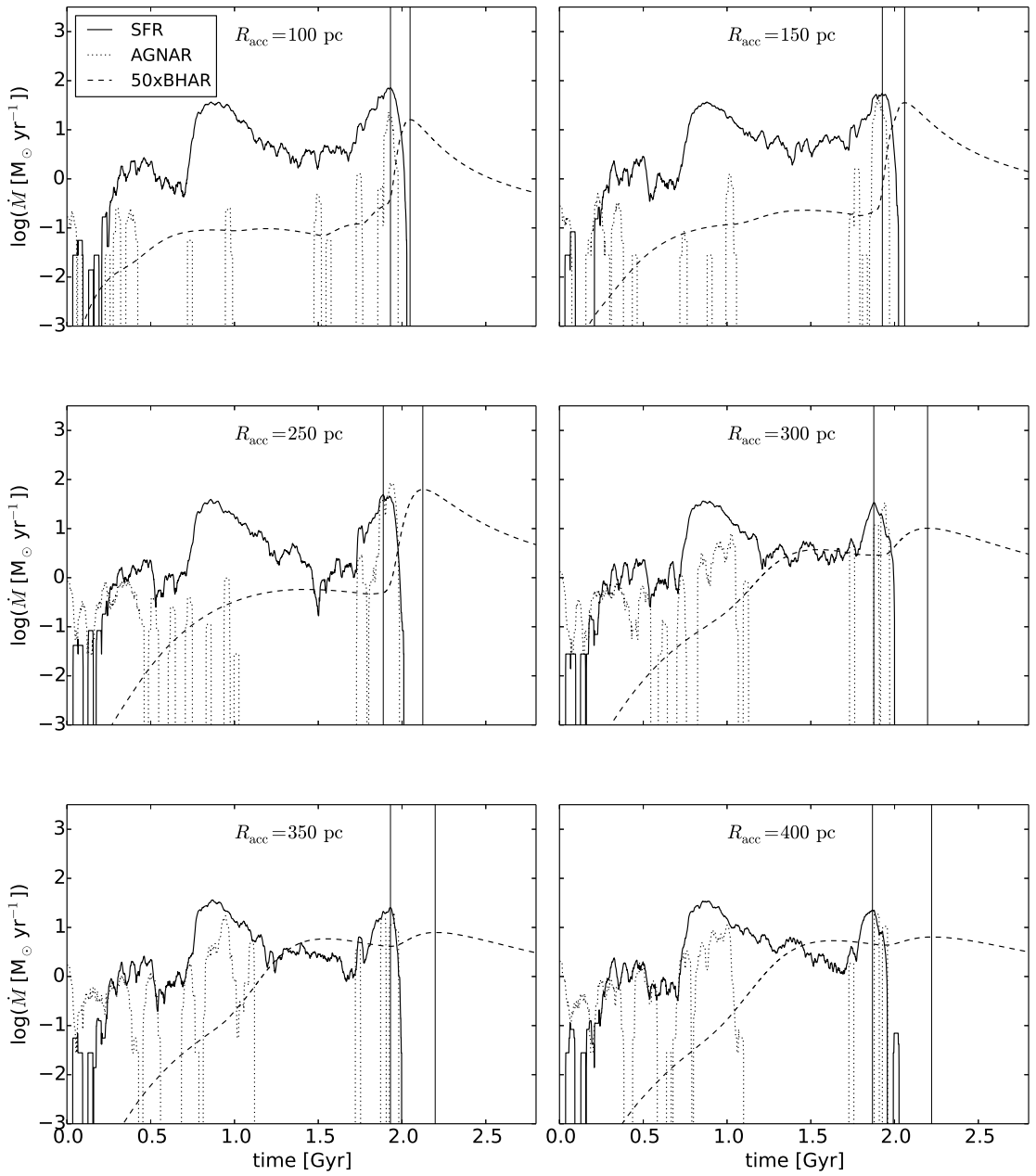

Figure 3. Star formation rate (SFR), accretion rate of the AGN (AGNAR) and black hole accretion rate (BHAR) as functions of time for different values of the accretion radius R_{acc}. The vertical lines mark the peak of the SFR and the peak of the BHAR, respectively.

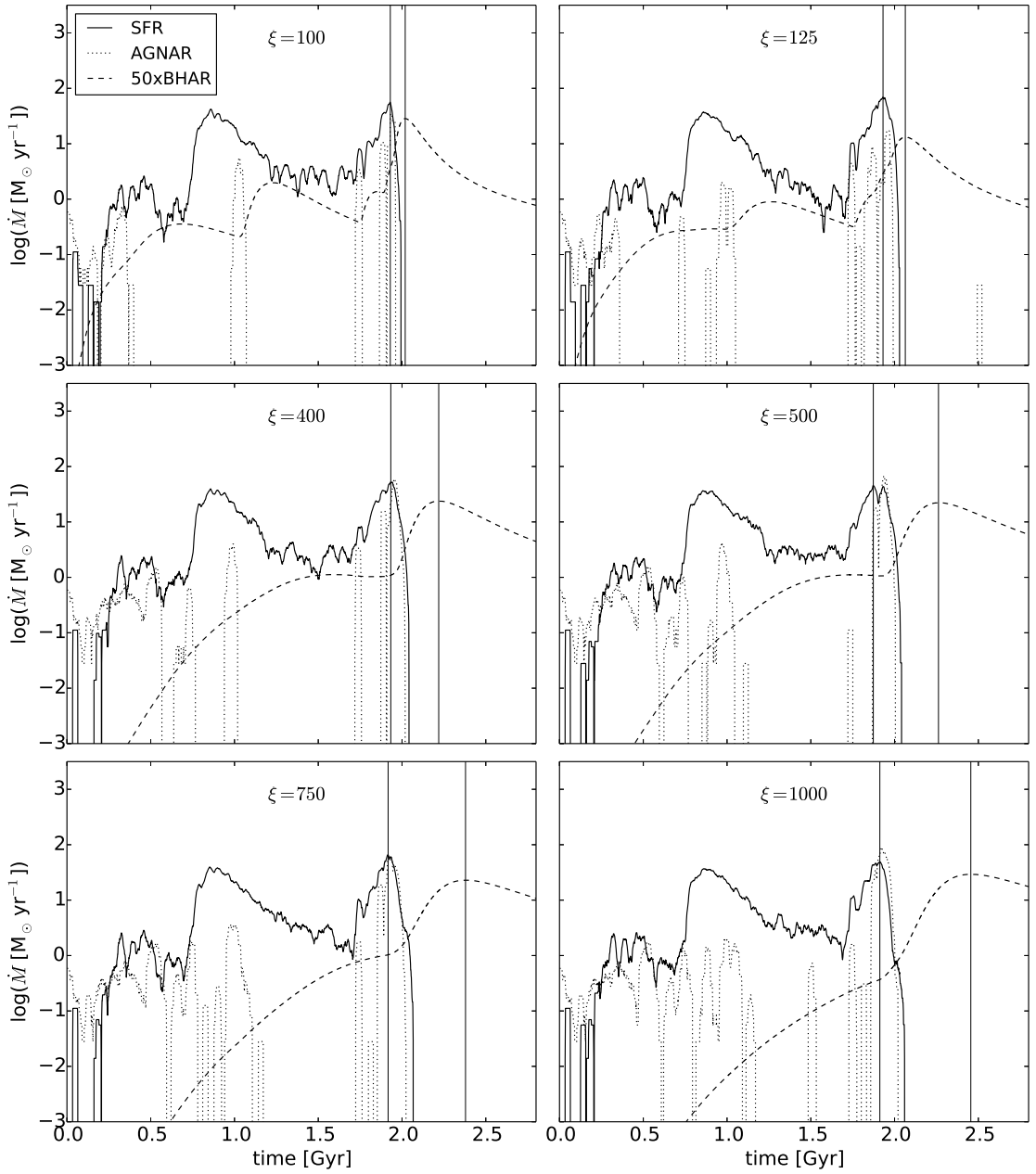

Figure 4. Star formation rate (SFR), accretion rate of the AGN (AGNAR) and black hole accretion rate (BHAR) as functions of time for different values of the viscosity parameter ξ. The vertical lines mark the peak of the SFR and the peak of the BHAR, respectively.

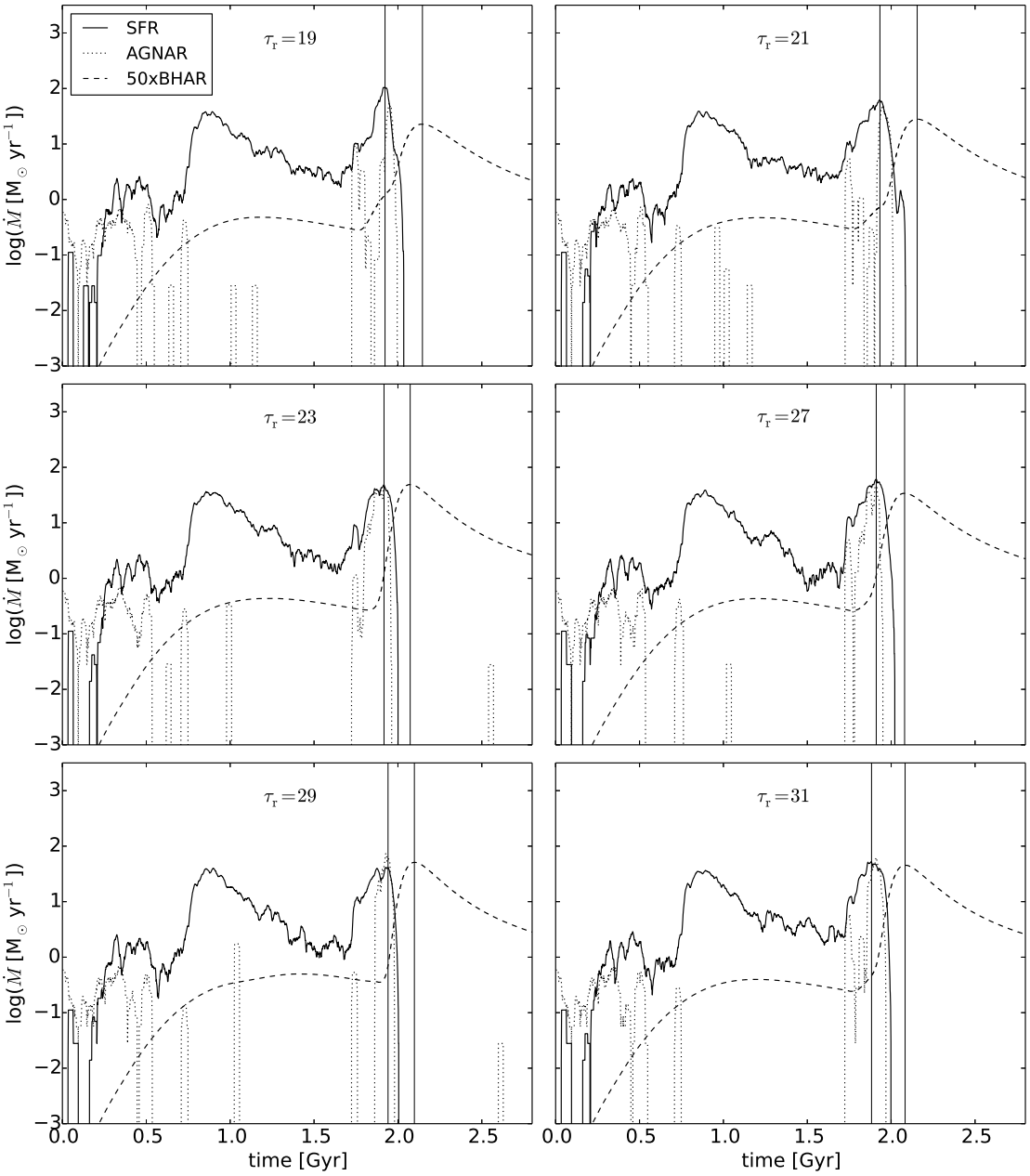

Figure 5. Star formation rate (SFR), accretion rate of the AGN (AGNAR) and black hole accretion rate (BHAR) as functions of time for different values of the feedback parameter τ_r. The vertical lines mark the peak of the SFR and the peak of the BHAR, respectively.

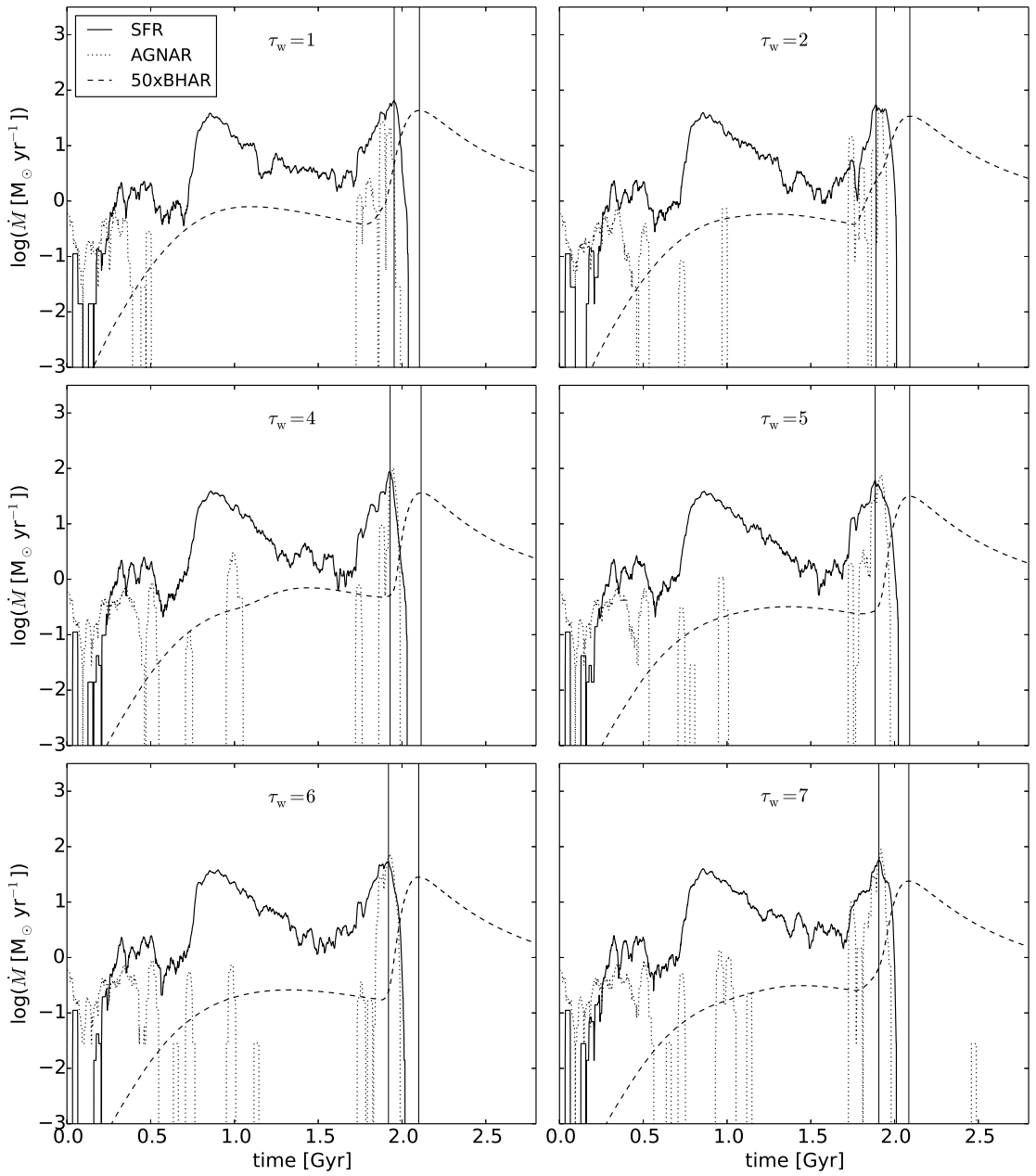

Figure 6. Star formation rate (SFR), accretion rate of the AGN (AGNAR) and black hole accretion rate (BHAR) as functions of time for different values of the feedback parameter τ_w. The vertical lines mark the peak of the SFR and the peak of the BHAR, respectively.

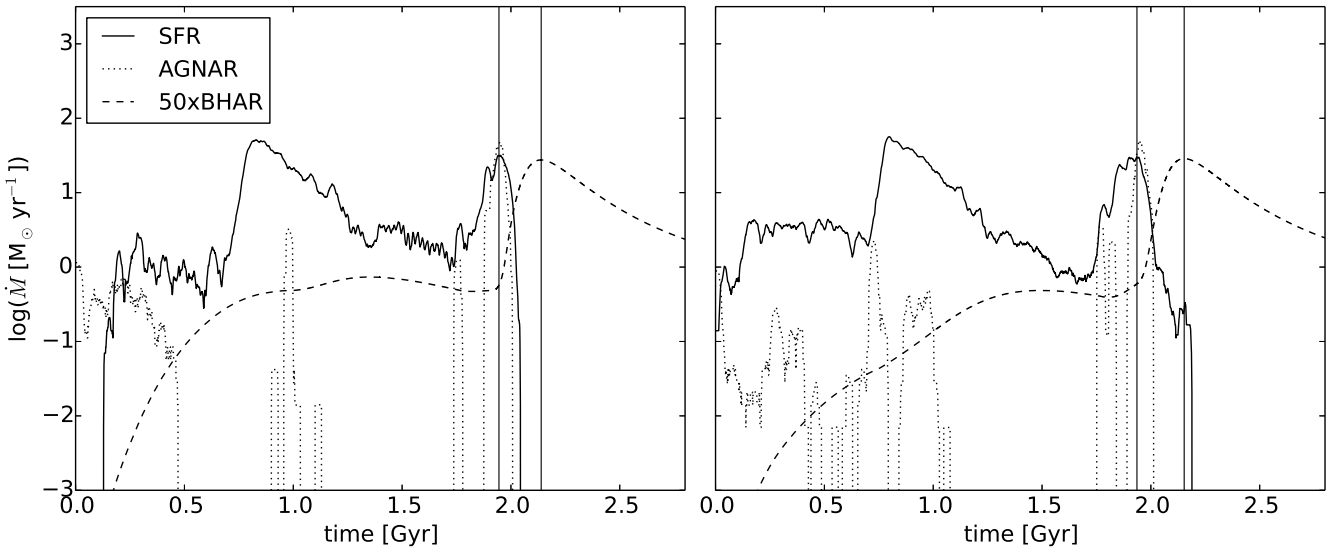

Figure 7. Star formation rate (SFR), accretion rate of the AGN (AGNAR) and black hole accretion rate (BHAR) as functions of time for different resolution levels. Left: particle number increased by a factor of two, right: particle number increased by a factor of four. The vertical lines mark the peak of the SFR and the peak of the BHAR, respectively.

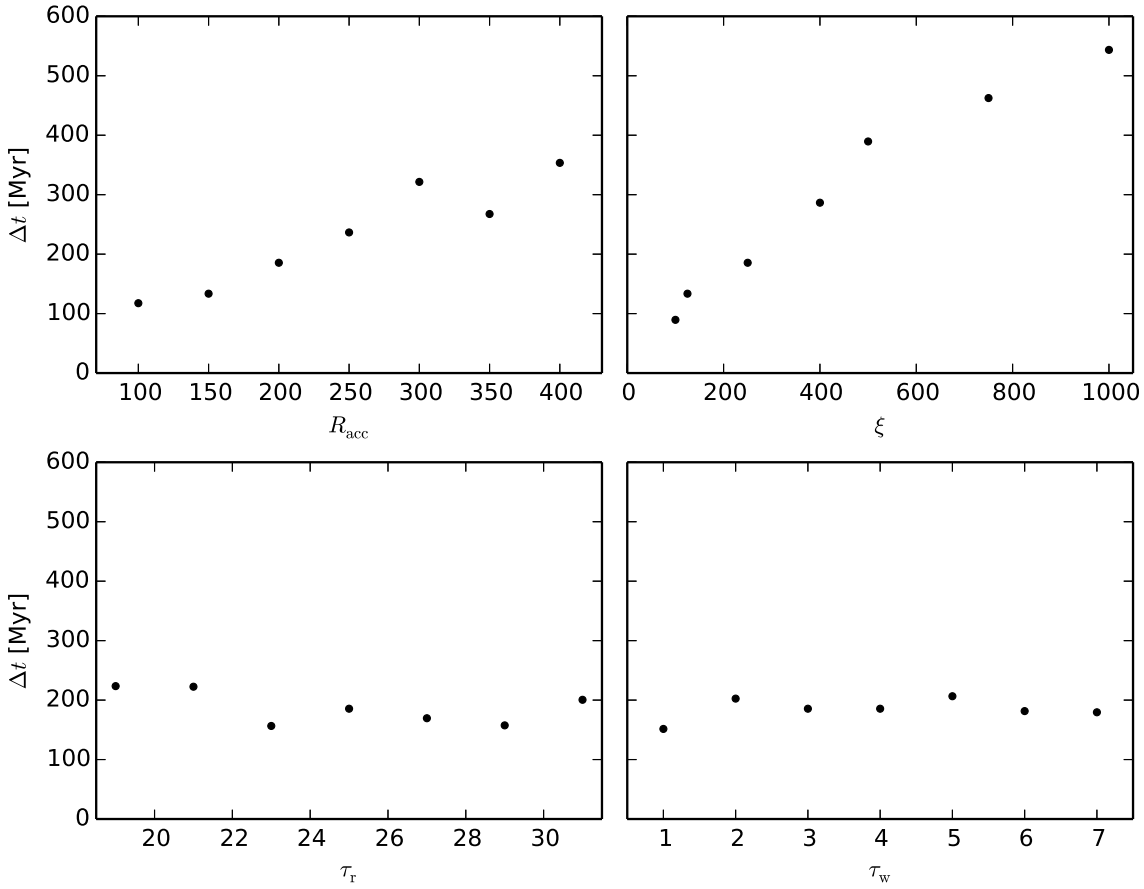

Figure 8. Time lag between starburst and AGN activity with the values of $R_{\rm acc}$, ξ, $\tau_{\rm r}$ and $\tau_{\rm w}$ from our parameterstudy (Table 2) and our reference model.

For the former resolution level the gravitational softening length for the halo particles is 0.64 kpc and 0.4 kpc for all other particles, for the latter resolution level the gravitational softening length for the halo particles is 0.5 kpc and 0.32 kpc for all other particles. Both resolution levels show the same features as our reference model: the simulations produce a starburst and a peak in the BHAR, and a time lag between these phenomena of about 200 Myr. However, there are still small differences between these simulations, to further reduce these deviations additional adjustments to the respective resolution levels would be necessary. For instance, Hopkins et al. (2013) argue that the critical density for the onset of star formation $\rho_{\rm crit}$ has to be adjusted for resolution. But as the above mentioned key features are already reproduced we refrain from such a fine tuning of our simulation parameters.

5 SUMMARY

With only one model setup we were able to reproduce three observational findings that have been identified in galaxies:

(i) The observed time lag between starburst and AGN activity is, in our work, principally caused by a viscous time lag the gas needs to flow through the AGN's accretion disc until it reaches the central black hole.

(ii) Our results match the observed $M_{\rm BH}$-σ correlation, but additionally include the aforementioned time lags. As, e.g., Di Matteo et al. (2005) or Debuhr et al. (2011) have already shown, AGN feedback is responsible for this relation.

(iii) The large scatter of the $M_{\rm BH}$-σ correlation is, in our work, caused by the continuing evolution of the black hole mass after the merging event.

The time lag does not only occur between starburst and AGN activity, but also between the peak in the AGNAR and the peak in the BHAR. Thus it is evident that this time lag is caused by the gas being delayed by the AGN particle, i.e. by the gas needing some time to move through the accretion disc. In addition our parameter study shows that the time lag increases with increasing size of the accretion disc, and decreases with increasing viscosity, indicating that it is indeed a viscous time-scale that delays the gas. Furthermore the parameter study shows that a time lag between starburst and AGN activity of the order of some 100 Myr can be reproduced for a wide range of parameters and for different resolution levels. Thus our conclusions do not depend on the detailed choice of the parameters, as long as they are taken from within a physically sensible range.

ACKNOWLEDGEMENTS

We thank Drs. Ralf Klessen, Volker Springel and Meng Xiang–Grüß for making available some of the numerical tools that we used for the calculations presented in this paper. We furthermore thank the referee for his comments on an earlier version of this paper, that significantly improved the quality of the publication.

REFERENCES

Beckert T., Duschl W. J., 2002, A&A, 387, 422
Crank J., Nicolson P., Hartree D. R., 1947, Proceedings of the Cambridge Philosophical Society, 43, 50
Davies R. I., Müller Sánchez F., Genzel R., Tacconi L. J., Hicks E. K. S., Friedrich S., Sternberg A., 2007, ApJ, 671, 1388
Debuhr J., Quataert E., Ma C.-P., 2011, MNRAS, 412, 1341
Debuhr J., Quataert E., Ma C.-P., 2012, MNRAS, 420, 2221
Di Matteo T., Springel V., Hernquist L., 2005, Nature, 433, 604
Duschl W. J., Strittmatter P. A., Biermann P. L., 2000, A&A, 357, 1123
Eddington A. S., 1921, Z. Phys., 7, 351
Gebhardt K., Bender R., Bower G., Dressler A., Faber S. M., Filippenko A. V., Green R., Grillmair C., Ho L. C., Kormendy J., Lauer T. R., Magorrian J., Pinkney J., Richstone D., Tremaine S., 2000, ApJ, 539, L13
Gültekin K., Richstone D. O., Gebhardt K., Lauer T. R., Tremaine S., Aller M. C., Bender R., Dressler A., Faber S. M., Filippenko A. V., Green R., Ho L. C., Kormendy J., Magorrian J., Pinkney J., Siopis C., 2009, ApJ, 698, 198
Hernquist L., 1993, ApJ, 409, 548
Hopkins P. F., 2012, MNRAS, 420, L8
Hopkins P. F., Narayanan D., Murray N., 2013, MNRAS, 432, 2647
Jappsen A.-K., Klessen R. S., Larson R. B., Li Y., Mac Low M.-M., 2005, A&A, 435, 611
Johansson P. H., Naab T., Burkert A., 2009, ApJ, 690, 802
Katz N., 1992, ApJ, 391, 502
Katz N., Weinberg D. H., Hernquist L., 1996, ApJS, 105, 19
Kennicutt Jr. R. C., 1998, ApJ, 498, 541
Khochfar S., 2003, PhD thesis, University of Heidelberg
Kormendy J., Richstone D., 1995, ARA&A, 33, 581
Mo H. J., Mao S., White S. D. M., 1998, MNRAS, 295, 319
Navarro J. F., Frenk C. S., White S. D. M., 1996, ApJ, 462, 563
Navarro J. F., Frenk C. S., White S. D. M., 1997, ApJ, 490, 493
Power C., Nayakshin S., King A., 2011, MNRAS, 412, 269
Pringle J. E., 1981, ARA&A, 19, 137
Salpeter E. E., 1964, ApJ, 140, 796
Scannapieco C., Tissera P. B., White S. D. M., Springel V., 2005, MNRAS, 364, 552
Schawinski K., Virani S., Simmons B., Urry C. M., Treister E., Kaviraj S., Kushkuley B., 2009, ApJ, 692, L19
Shakura N. I., Sunyaev R. A., 1973, A&A, 24, 337
Springel V., 2000, MNRAS, 312, 859
Springel V., 2005, MNRAS, 364, 1105
Springel V., Di Matteo T., Hernquist L., 2005, MNRAS, 361, 776
Springel V., Hernquist L., 2003, MNRAS, 339, 289
Springel V., White S. D. M., 1999, MNRAS, 307, 162
Wild V., Heckman T., Charlot S., 2010, MNRAS, 405, 933
Wurster J., Thacker R. J., 2013, MNRAS, 431, 539

This paper has been typeset from a TEX/ LATEX file prepared by the author.